Factors Limiting Convective Cloud-Top Height at the ARM Nauru Island Climate Research Facility

MICHAEL P. JENSEN*

Department of Applied Physics and Applied Mathematics, Columbia University, and NASA Goddard Institute for Space Studies, New York, New York

ANTHONY D. DEL GENIO

NASA Goddard Institute for Space Studies, New York, New York

(Manuscript received 2 May 2005, in final form 11 October 2005)

ABSTRACT

Cumulus congestus clouds, with moderate shortwave albedos and cloud-top temperatures near freezing, occur fairly often in the Tropics. These clouds may play an important role in the evolution of the Madden–Julian oscillation and the regulation of relative humidity in the midtroposphere. Despite this importance they are not necessarily simulated very well in global climate models. Surface remote sensing observations and soundings from the Atmospheric Radiation Measurement (ARM) climate research facility at Nauru Island are coupled with a simple parcel model in order to address the following questions about these cloud types: 1) Which environmental factors play a role in determining the depth of tropical convective clouds? 2) What environmental parameters are related to entrainment rate in cumulus congestus clouds? The results presented herein suggest that at Nauru Island a drying of the midtroposphere is more likely to be responsible for limiting congestus cloud-top heights than is a stabilizing of the freezing level. It is also found that low-level CAPE and the RH profile account for the largest portion of the variance in cumulus congestus entrainment rates, consistent with the idea that entrainment rate depends on the buoyant production of turbulent kinetic energy. If the analysis is limited to cases where there is a sounding during the hour preceding the cumulus congestus observations, it is found that the low-level CAPE accounts for 85% of the total variance in entrainment rate.

1. Introduction

To model the energetic effects of clouds in the earth's atmosphere we must better understand cloud characteristics such as cloud type, cloud dimensions, and cloud microphysics and how these variables relate to the atmospheric state and large-scale dynamics. Tropical convective clouds are an obvious feature in satellite images of tropical latitudes due to their high shortwave albedos; however, depending on the atmospheric state and large-scale dynamics, different convective cloud types can develop with vastly different impacts on the local water and energy budgets.

Shallow trade cumulus and stratocumulus are very bright in the shortwave, but show little perturbation to the upwelling longwave flux. Their cloud-top heights are limited by the depth of the boundary layer. Deep convective cloud systems may have shortwave albedos as high as 70% (McFarquhar and Heymsfield 1996) and infrared (IR) brightness temperatures near 200 K. A third mode in the frequency distribution of tropical convective cloud types is represented by cumulus congestus (Johnson et al. 1999), which have moderate shortwave albedos and cloud-top temperatures near freezing. The type of convective cloud that occurs under a given set of environmental conditions will have consequences for the redistribution of radiative and latent heating through the depth of the troposphere. For climate model applications it is therefore important to understand the factors that determine the type of convective cloud that will occur.

* Current affiliation: Environmental Sciences Department, Brookhaven National Laboratory, Upton, New York.

Corresponding author address: Dr. Michael P. Jensen, Brookhaven National Laboratory, ESD/ESSD, Bldg. 490D, Upton, NY 11973-5000.
E-mail: mjensen@bnl.gov

In this study we concentrate on describing the factors that limit the cloud-top heights of midlevel cumulus congestus clouds preventing them from growing into deep convective clouds. Midlevel cumulus congestus clouds are characterized by cloud-base heights near the lifting condensation level, cloud-top heights near the freezing level (~5 km in the Tropics), a lack of ice hydrometeors, and measurable precipitation reaching the ground. Previous studies suggest that cumulus congestus cloud tops are limited by either the entrainment of dry air from above the boundary layer or by the loss of buoyancy of rising parcels as they encounter a weak stable layer near the freezing level.

Redelsperger et al. (2002) offer a rather complete summary of the different conditions that have been suggested to explain the limitation of cloud-top height in the case of cumulus congestus clouds. Three main explanations are offered. 1) The difference in cloud depth is a function of the environmental convective available potential energy (CAPE), 2) the buoyancy of congestus cloud elements is limited by weak stable layers, and/or 3) congestus cloud tops are limited by entrainment of dry environmental air above the boundary layer. Takemi et al. (2004), based on sensitivity tests with a cloud-resolving model, suggest that dry air at middle and upper levels is the most important limiting factor.

There has been a great deal of research aimed at understanding the structure of tropical deep convective systems (cf. Houze 1989). The stratiform region of the cloud system is characterized by ice particles growing by vapor deposition as they fall slowly through a mesoscale updraft region in the upper portion of the cloud. As the particles fall below the −12°C level, they aggregate and form larger snowflakes (Houze and Churchill 1987). A radar bright band is generally observed as these snowflakes then fall through the melting layer (approximately 4–5 km in the Tropics) and begin to melt. The heat required to melt the hydrometeors is removed from the air at the freezing level and as the anvil cloud dissipates this cooler layer remains and is manifest as a weak stable layer (Johnson et al. 1999). Mapes and Zuidema (1996) have also shown that changes in the vertical profile of static stability can result from radiational cooling near the bases of dry layers in the atmosphere. Convective parcels rising to the level of this weak stable layer will encounter a decrease in buoyancy. Since tropical convective parcels generally do not have a great deal of buoyancy, they may not be able to overcome even this weak stable layer and it may therefore act as a limitation on convective cloud growth.

The presence of layers of extremely dry air in the tropical midtroposphere has been noted by several investigators and the explanation of their origin was a major research topic for the Tropical Ocean Global Atmosphere Coupled Ocean–Atmosphere Response Experiment (TOGA COARE) field experiment. These intrusions of dry air have been found to occur on synoptic scales (Mapes and Zuidema 1996) with horizontal length scales on the order of a few hundred kilometers and time scales on the order of 3–4 days. The layers of dry air typically have bases at 1.5–2.0 km above the surface (DeMott and Rutledge 1998). Several investigators (Sheu and Liu 1995; Mapes and Zuidema 1996; Johnson et al. 1999; Yoneyama and Parsons 1999) have identified the source of these dry air intrusions to be advection of subtropical air; however, the processes responsible for these events are not well understood and several different dynamical mechanisms have been proposed (Numagati et al. 1995; Sheu and Liu 1995; Mapes and Zuidema 1996; Yoneyama and Parsons 1999). As mentioned above, these dry layers may affect the profile of static stability through radiational cooling near their bases. The buoyancy may also be affected by direct entrainment of the dry air and evaporation in the penetrating moist convection (Mapes and Zuidema 1996; Brown and Zhang 1997; DeMott and Rutledge 1998). Periods of dry air intrusions are characterized by a lack of clouds with infrared brightness temperatures less than 210 K, but do show a broad distribution of IR brightness temperature between 230 and 280 K (Brown and Zhang 1997). Thus, convective clouds do occur during these periods; however, they tend to be limited to midlevel cloud-top heights.

The potentially important role of dry air entrainment for the creation of cumulus congestus presents a serious problem for general circulation models (GCMs), whose cumulus parameterizations tend to underestimate the occurrence of all but deep convective clouds. Entrainment rates in GCM parameterizations are usually specified either in an ad hoc fashion or are calculated iteratively to produce neutral buoyancy in a spectrum of rising plumes at discretized model levels. Several attempts to parameterize entrainment physically have appeared (cf. the discussion in Gregory 2001), but few observational constraints exist. This limits both our ability to predict the presence of congestus, which may be a precursor to deep convection in some situations, and to estimate the updraft speeds of deep convective events, which affect the microphysical and radiative properties of cumulus anvils (Del Genio et al. 2005).

Recent work as part of the European Cloud Systems Study (EUROCS) has highlighted the prolems GCMs have in simulating the growth of convective cloud systems from shallow cumulus to midlevel cumulus congestus and finally to deep convection. Derbyshire et al. (2004) compare the results of two cloud resolving mod-

els (CRMs) and six single-column models (SCMs). They show that the SCMs fail to simulate the connections between free-tropospheric relative humidity and the presence of shallow convective clouds that is apparent in the CRMs. Guichard et al. (2004) show that while CRMs predict a progressive growth in the depth of convective clouds, SCMs simulate the instantaneous growth of deep convective clouds. These differences highlight the need for a better understanding of the factors that control the development of the spectrum of convective cloud types.

In this study we use data from the Atmospheric Radiation Measurement (ARM) climate research facility at Nauru Island (0.5°S, 166.9°E; Mather et al. 1998) to investigate the role that each of these mechanisms plays in limiting convective cloud-top heights. In section 2 of this paper the data sources are described. Section 3 describes the background and methods used in this study including the calculation of the convective available potential energy, the level of neutral buoyancy, and the estimation of entrainment rate. In section 4 we test two hypotheses concerning the processes that limit convective cloud growth. In section 5 the sensitivity of our results and conclusions to some of the simplifying assumptions is presented. In section 6 we investigate the relationship between several environmental parameters and the entrainment rate. We summarize our findings in section 7.

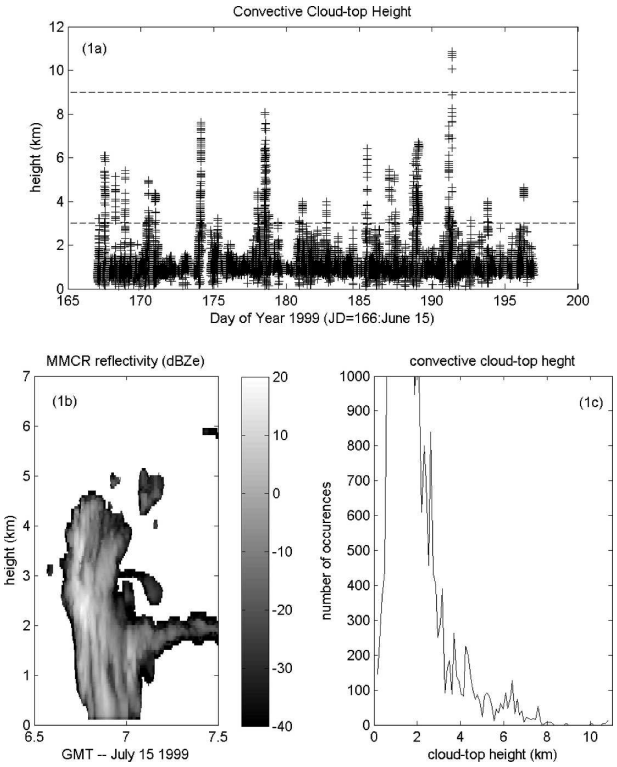

FIG. 1. Summary of convective cloud characteristics during the ARM Nauru99 intensive operation period. (a) Time series of convective cloud-top heights, where convective clouds are defined as those with cloud-base height below 2 km. (b) Millimeter cloud radar reflectivity for one example of a cumulus congestus cloud during Nauru99. (c) Histogram of convective cloud-top heights during Nauru99 illustrating the congestus mode of convection.

2. Data

In this study we use 4 yr of data from the ARM facility at Nauru Island in the tropical western Pacific (TWP). The TWP ARM sites are designed to obtain continuous observations of surface meteorology, the atmospheric state, and the surface radiation budget (Mather et al. 1998) over climatically significant time scales. To obtain these observations a suite of surface-based remote sensing instruments is deployed. Most important to the goals of this study are a 35-GHz cloud radar and a micropulse lidar for defining cloud boundaries and structure, rawindsondes for defining the vertical structure of the atmosphere, and pyranometers/pyrgeometers for defining the downwelling radiative fluxes at the surface. The ARM facility at Nauru Island was established in November 1998 and was selected because it is on the eastern edge of the Pacific warm pool under La Niña conditions.

The ARM Active Remotely Sensed Cloud Locations (ARSCL) Product (Clothiaux et al. 2000) uses a combination of reflectivity measurements from the 35-GHz cloud radar and the micropulse lidar to describe the cloud boundaries and radar reflectivity. Recent studies (Kollias et al. 2003, 2006) have shown that the cloud radar is capable of the accurate detection of cloud-top heights even in thick precipitating clouds with rain rates less than 5 mm h^{-1} (P. Kollias 2005, personal communication). Since this is much greater than the rain rates we expect from cumulus congestus clouds, we are confident in the cloud-top height estimates from the ARSCL product.

Figure 1a shows the convective cloud-top heights for 16 June–15 July 1999 from the ARSCL datastream where we have defined convective events as observations with an ARSCL cloud-base height less than 2 km. This figure clearly shows the three modes of convective cloud occurrence discussed by Johnson et al. (1999). Boundary layer trade cumulus clouds are present throughout this entire period, and cumulus congestus clouds (tops near the freezing level ~5 km) are very common while deep convective clouds occur less frequently. Figure 1b shows the radar reflectivity profile for a typical cumulus congestus cloud. Note the cloud-top height near the freezing level and the presence of a

detrained stratus deck that coincides with the inversion-capped boundary layer (approx 2 km). To emphasize the modality of the convective cloud-top heights, Fig. 1c shows the histogram of the cloud-top heights from Fig. 1a. The vast majority of convective clouds are of the boundary layer variety (88%); however, there is a local maximum in the frequency distribution of cloud-top heights near 6 km and a general broadening in the 4–8-km bins (12%). Finally, there is a small local maximum (approx 10 km) in the right-hand wing of the distribution representing the deep convective clouds (<1%).

To investigate the importance of the processes summarized by Redelsperger et al. (2002), we use radiosonde profiles from Nauru to describe the environmental thermodynamic structure in which convection forms. The Vaisala RS80 radiosondes used at Nauru suffer from a well-documented dry bias that has been traced to the contamination of the humidity sensor by its packaging (Guichard et al. 2000; Wang et al. 2002; Westwater et al. 2003). We have applied a correction to account for this dry bias based on the work of Wang et al. (2002).

We use the ARSCL product to identify cumulus congestus cases using the definition of cloud-base height below 1 km and cloud-top height between 3 and 9 km. The choice of 9 km as the breakpoint allows for overshooting of the freezing level by cumulus congestus clouds and is consistent with the criteria used by Johnson et al. (1999). Over the time period from January 1999 through December 2002 the cloud radar is operational for approximately 870 days. We further limit our analysis to cases with a sounding launch during the preceding 6 h assuming that profiles observed earlier than that would not be representative of the environment in which the convection occurred. Using these definitions of cumulus congestus, we define a total of 67 cases to include in our analysis.

3. Thermodynamic analysis

We analyze the data with a simple parcel model in order to investigate the importance of CAPE, stable layers, and dry intrusions in limiting convective cloud-top heights.

a. Convective available potential energy

CAPE can be thought of as the amount of buoyant energy available for the vertical acceleration of an undiluted air parcel. The greater the value of CAPE, the higher the upper limit on updraft vertical velocity during cloud and storm growth, although deceleration due to entrainment, vertical pressure gradients, and water loading prevents this limit from being realized. The "shape" of the CAPE may also have a significant impact on the observed updraft velocities (Lucas et al. 1994; Blanchard 1998). The total value of CAPE is a function of the vertical distribution of buoyancy and the depth of the free convective layer (Blanchard 1998). In investigating the reasons that convection over the ocean has weaker updrafts than continental convection, Lucas et al. (1994) distinguish between "fat" CAPE profiles, which have a great deal of buoyancy at low levels and a lower level of neutral buoyancy, and "skinny" profiles, which have small buoyancy but through a much greater depth. These two different profile types result in different vertical velocity profiles especially in the lower and middle troposphere. When considering cumulus congestus clouds, we are interested in the factors that affect the low- and midlevel vertical velocity and therefore we will limit our calculation of CAPE to the lowest 5 km (for simplicity we refer to this as the low-level CAPE). Figure 2 shows a scatter diagram of the ARSCL cloud-top height for the cumulus congestus versus the natural logarithm of the low-level CAPE from the nearest preceding sounding. We have also included the mean of the ARSCL cloud-top height for 0.5 ln (low-level CAPE) bins with the corresponding standard deviation indicated by the error bars. This plot shows a hint of a relationship between increasing low-level CAPE and increasing convective cloud-top height; however, this signal is well within the noise and no clear relationship can be discerned. This is consistent with the conclusions of Redelsperger et al. (2002) who show similar cloud-top

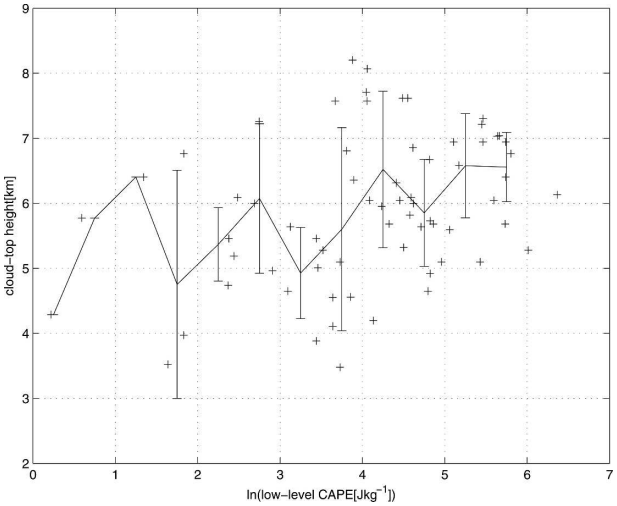

FIG. 2. The ln (low-level CAPE) vs ARSCL cloud-top height for the 67 cumulus congestus cases observed at Nauru. The solid line represents the mean cloud-top height for 0.5 ln (CAPE) bins with the std dev in each bin noted by the error bars.

heights resulting in similar environmental CAPE conditions during TOGA COARE. Sherwood (1999) showed that although there is a minimum amount of CAPE necessary for convection to occur in the Tropics, increased CAPE does not necessarily result in more vigorous convection.

The absolute value of CAPE is very sensitive to the definition of the initial characteristics of the rising parcel. For the analysis above we have chosen the median thermodynamic properties in the lowest 1 km (as an approximation of the typical boundary layer properties) to define the initial characteristics of the parcel. We could have also used the thermodynamic characteristics at 1000 mb, or any of several different heights or average values to define the initial characteristics. Because we are unsure of exactly where the convective parcels are originating from, we do not have a physical means from which to determine these characteristics. Therefore, we will test the sensitivity of our conclusions to different definitions of the initial parcel characteristics in section 5.

b. Level of neutral buoyancy

We use a modified parcel theory to evaluate the effect of the environmental temperature and humidity profiles on cloud-top height. For pseudoadiabatic ascent (i.e., upon condensation, water is immediately removed from the parcel through precipitation) the temperature of the parcel is determined by the conservation of equivalent potential temperature (θ_e). A parcel begins with $\theta_{ep}(z_0) < \theta_{es}(z_0)$ (the subscript p indicates θ_e for the parcel and θ_{es} is the saturated equivalent potential temperature). As the parcel rises, conserving θ_{ep}, it will eventually reach a level where $\theta_{ep}(z_{LFC}) = \theta_{es}(z_{LFC})$; this is the level of free convection (LFC). As the parcel rises above the LFC, it is positively buoyant and will continue to rise until eventually $\theta_{ep}(z_{LNB}) = \theta_{es}(z_{LNB})$ again; this is the level of neutral buoyancy (LNB). The parcel may rise slightly above the LNB but it then becomes negatively buoyant and returns to the LNB. Figure 3 shows an example sounding from Nauru with the LNB indicated. We take this as the approximate cloud-top height for undiluted ascent. In section 5 we will test the sensitivity of our results to the assumption of moist adiabatic ascent.

c. Estimating the entrainment

In reality, the ascent of a convective parcel is modulated by the entrainment of environmental air and water loading, resulting in a decrease of its buoyancy and its LNB. (We designate the level of neutral buoyancy of an entraining parcel as ELNB to distinguish it from the adiabatic case.)

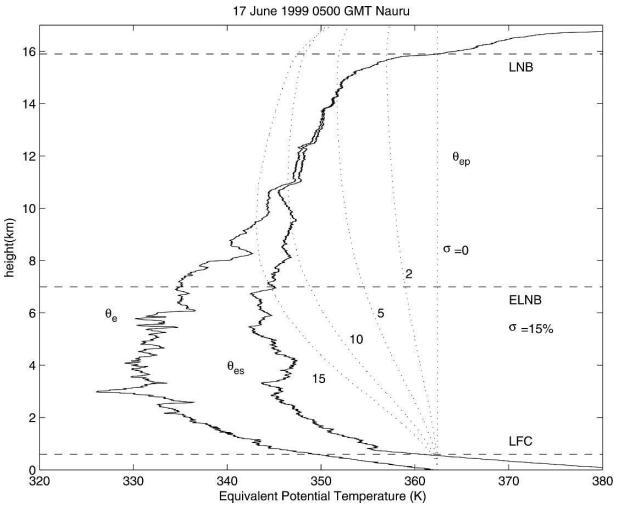

FIG. 3. Plots of the environmental θ_e and θ_{es} (solid) for the 0500 UTC 17 Jun 1999 sounding from Nauru99 with θ_{ep} for entrainment rates of 0%, 2%, 5%, 10%, and 15% km^{-1}. The LNB and ELNB(σ = 15%) are indicated by the horizontal dashed lines.

To estimate the entrainment of environmental air for each of the cumulus congestus cases, we assume for simplicity a constant entrainment rate with height (Brown and Zhang 1997) and determine a new profile of θ_{ep} where

$$\theta_{ep}(z + \Delta z) = \left[\frac{\theta_{ep}(z) + \sigma \Delta z \theta_e}{(1 + \sigma \Delta z)}\right], \qquad (1)$$

where σ is the entrainment rate (% km^{-1}) and Δz (km) is the change in height of the parcel. From this new profile of θ_{ep}, the ELNB is determined. We determine σ iteratively, starting with a value of 0.1% km^{-1} and increasing it in steps of 0.1% km^{-1} until the new ELNB is approximately equal to the ARSCL cloud-top height. Figure 3 shows profiles of θ_{ep} and the resulting ELNB for several different entrainment rates between 0% and 15%. Using this method, we estimate values of entrainment ranging between 1% and 68% km^{-1} for the 67 cases from Nauru. Figure 4 shows a scatterplot of the ARSCL cloud-top height versus the estimated entrainment rate with the mean entrainment rate in 1-km cloud-top height bins indicated by the solid line. On average, entrainment rates are approximately constant for cloud-top heights up to the midtroposphere, then decreasing entrainment rates are required to get higher cloud-top heights. The scatter is likely related to our assumption of constant entrainment rate with height, varying details of the thermodynamic profile, variable water loading, the effects of freezing of cloud particles, basic limitations of the parcel theory analysis, and unresolved changes in thermodynamic structure between the time of the sounding and the ARSCL observation.

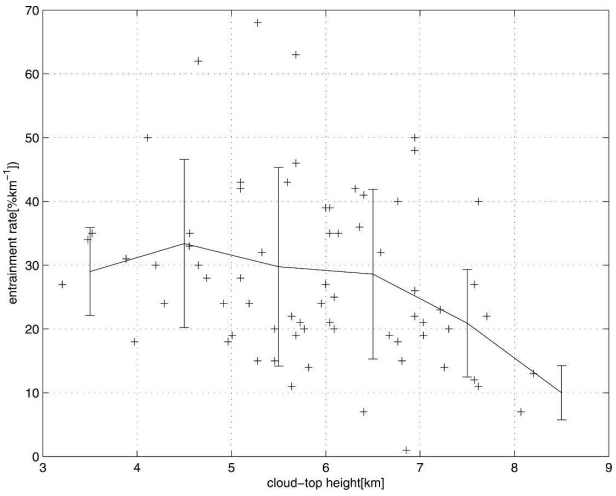

FIG. 4. ARSCL cloud-top height vs estimated entrainment rate. The solid line represents the mean entrainment rate for 1000-m cloud-top height bins with the standard deviation in each bin noted by the error bars.

4. Hypothesis testing

a. Hypothesis 1—Climatological thermodynamics

Once we have estimated the entrainment rate for each convective cloud case we can explore how changes in the thermodynamic characteristics of the environment affect the calculated ELNB. These changes can then be interpreted in the context of the mechanisms for limiting convective cloud growth summarized by Redelsperger et al. (2002). We first pose the testable hypothesis that a climatological thermodynamic profile is conducive to the growth of cloud-top heights to deep convective levels (i.e., >9 km). We define a "climatological" thermodynamic profile by taking the mean temperature and relative humidity over all profiles obtained at Nauru between January 1999 and December 2002. The mean sounding is determined by first smoothing each sounding to 20-m vertical height bins and then taking the mean over all the smoothed soundings at each height. Figure 5 shows a comparison of the climatological profiles of stability and relative humidity to a mean of the cumulus congestus cases. We note that the congestus soundings are generally more humid through the depth of the troposphere and more unstable below 2.5 km (but more stable from 2.5 to 5 km) compared to climatological conditions. The climatological temperature profile is then substituted for each cumulus congestus profile while holding the relative humidity profile constant, and vice versa. We then calculate a new ELNB, assuming that the entrainment rate from our original estimate is still appropriate (a decrease in the entrainment rate in itself will increase the ELNB).

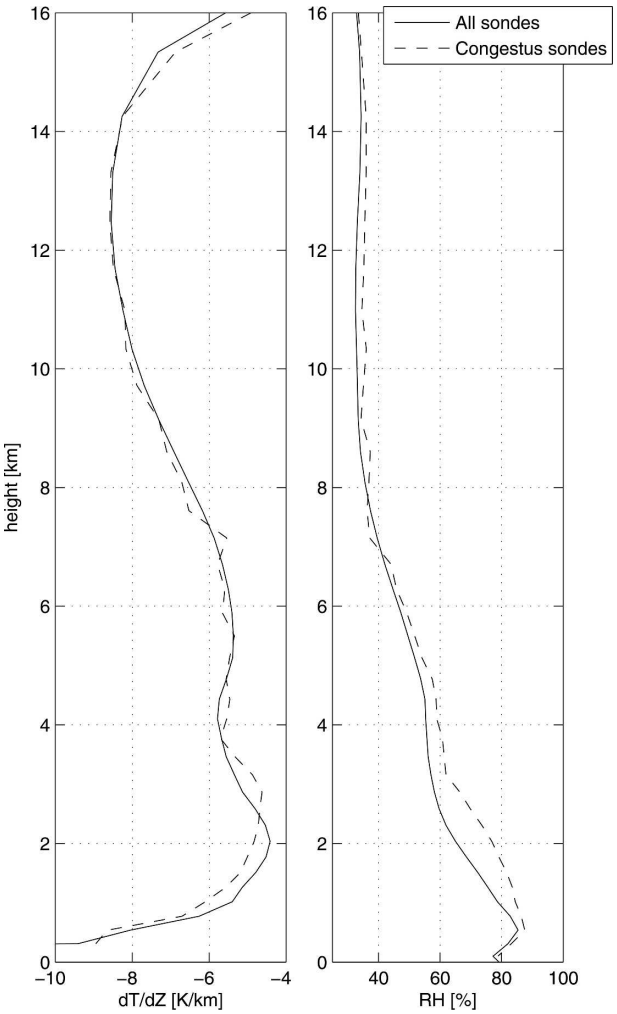

FIG. 5. Comparison of the stability (dT/dZ) and RH for the mean of all soundings taken at Nauru to the mean of the 67 congestus cases identified in this study.

Figure 6a summarizes the results as a function of the midlevel relative humidity. For the substitution of the climatological temperature profile (circles), 21 cases show a decrease in the ELNB while 46 cases show an increase in the ELNB. The mean increase in ELNB for the 46 cases that show an increase is 1.44 km (median 1.14 km) resulting in only 3 cases where the ELNB has increased to deep convective levels. The increase in the ELNB tends to be slightly greater for larger midlevel RH. For the substitution of the climatological relative humidity profile (Xs), 45 cases show a decrease in the ELNB while 22 cases show an increase. The mean increase in ELNB for these 22 cases is 2.88 km (median 1.85 km) with only 5 cases where the ELNB has increased to deep convective levels. As the midlevel RH increase, there are fewer cases that reach deep convective levels and the increase in ELNB is smaller. This is

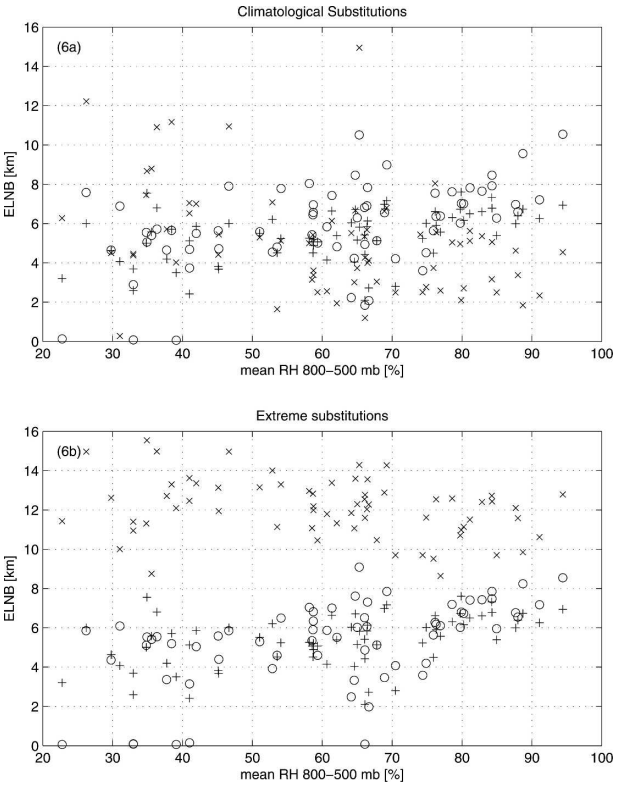

FIG. 6. ELNB as a function of midlevel relative humidity for each sounding (+) and for the substitution of (a) climatological temperature (circle) and relative humidity (X) and (b) temperature profile of a sounding that is unstable near the freezing level (circle) and the relative humidity profile of a sounding with a moist midlevel (X).

consistent with the profiles in Fig. 4 as the dry conditions that are typical at Nauru are more conducive to development of shallow trade cumulus. Thus, the climatological structure at Nauru is not conducive for the growth of a deep convective cloud.

b. *Hypothesis 2—Extreme thermodynamics*

We next test whether convective cloud-top heights are limited by the presence of weak stable layers near the freezing level and/or dry air just above the freezing level. Since the Nauru data record includes convective clouds of all types, and it will include thermodynamic profiles consistent with the development of deep convective systems, we search the Nauru soundings for a case without a stable temperature profile near the freezing level (extreme T) and a case with a relatively high midlevel relative humidity (extreme RH). Following the same procedure as in section 4a, we use the estimated entrainment rates (from 3c) and calculate the ELNB for each case after the substitution of the extreme temperature profile while holding the RH profile constant and vice versa.

Figure 6b shows that for the substitution of the sounding with low freezing-level stability (circles) 39 of the 67 congestus cases show an increase in the ELNB. (The 28 cases that show a decrease are due to their most stable layers being at a different height than the extreme T profile.) The mean increase in ELNB for these cases is 1.04 km (median 1.88 km) and just one of the cases shows an increase to deep convective levels. There is a slight trend to larger increases in the ELNB with increasing midlevel RH. For the substitution of the RH from the sounding with high midlevel RH (Xs), all 67 cases show an increase in the ELNB. The mean increase in ELNB is 6.81 km (median 6.94 km) with 64 of the 67 cases showing values of ELNB greater than 9 km. The magnitude of the increase in ELNB decreases as the midlevel RH increases. These results are consistent with the cloud resolving model sensitivity tests conducted by Takemi et al. (2004).

5. Sensitivity tests

The preceding analysis suggests that for cumulus congestus clouds at Nauru, the midlevel humidity plays a more significant role in suppressing the growth of deep convective clouds than the stability near the freezing level, though in some cases the stability is also important. In coming to this conclusion we have made several important assumptions, for example, pseudoadiabatic ascent, the origin level of convective parcels, and constant entrainment rate with height. We next investigate the sensitivity of our results to these assumptions.

a. *Pseudo- versus moist-adiabatic ascent*

To this point we have assumed pseudoadiabatic ascent; that is, condensed water is immediately removed from the parcel. Alternatively, we could have assumed that the ascent was moist adiabatic by retaining all condensed water in the parcel. In reality convective processes likely exhibit behavior that is intermediate between these two extremes. However, these simple processes should offer bounds to the range of the actual LNB and entrainment rates. We follow the procedure of Xu and Emanuel (1989) in order to define the moist-adiabatic ascent of a parcel.

For a given thermodynamic profile, a parcel rising via pseudoadiabatic ascent will have greater buoyancy at any given height than a similar parcel rising via moist-adiabatic ascent (Xu and Emanuel 1989) and therefore will also have a higher ELNB. Thus, for a given ARSCL cloud-top height, our estimated entrainment rate will be greater for pseudoadiabatic ascent compared to moist-adiabatic ascent. Figure 7 shows a com-

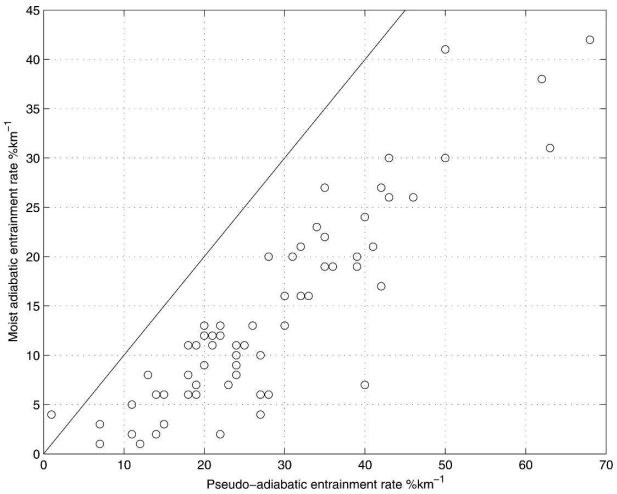

FIG. 7. Estimated entrainment rate assuming pseudoadiabatic ascent vs moist-adiabatic ascent.

parison of the estimated entrainment rate assuming pseudoadiabatic and moist-adiabatic ascent. The entrainment rates for pseudoadiabatic ascent range between 1% and 68% km^{-1} while for moist-adiabatic ascent this range is 1% to 43% km^{-1}. The differences between these entrainment rates range from 4% to 33% km^{-1} over the 67 cases with a mean difference of 14.0% km^{-1} (median 13% km^{-1}).

Table 1 compares the cloud-top heights obtained for pseudoadiabatic and moist-adiabatic ascent for the various thermodynamic profile assumptions used in section 4. The values in the first four rows of the table summarize the results shown in Fig. 6 for pseudoadiabatic ascent. For the substitution of the climatological temperature profile the moist-adiabatic case shows a slightly greater inclination for clouds to grow to deep convective cloud depths. While fewer cases show an increase in ELNB (33 compared to 46 for pseudoadiabatic), there are a greater number of cases reaching ELNB $>$ 9 km (eight compared to three) and a larger mean increase (by approx 1 km) in ELNB. For the climatological relative humidity there are two more cases that show an increase in the ELNB for moist-adiabatic ascent (24 compared to 22) and of those that increase, seven reach deep convective heights compared to five for pseudoadiabatic ascent. Although there are some small differences, regardless of the type of ascent that is assumed, only a small fraction of the cases reach deep convective heights upon substitution of the climatological profiles, and therefore our conclusions regarding climatological conditions remain valid. For the substitution of the sounding with low freezing-level stability (ExT), fewer cases show an increase in the ELNB for moist-adiabatic (32) compared to the pseudoadiabatic cases (39) with seven cases reaching 9 km. For the substitution of the RH from the sounding with a moist midlevel, most of the cases show increases to greater than 9 km regardless of the ascent type. The increase in mean ELNB is 0.7 km larger for the moist-adiabatic analysis. When comparing the different rows in Table 1, it is important to keep in mind that for each parcel ascent type we have estimated a new entrainment rate. While we would expect the increase in ELNB for the ExT and ExRH substitutions to be smaller for moist-adiabatic ascent (due to the decreased buoyancy from water loading) for the same entrainment rate, this is not necessarily true with our recalculated entrainment rates. On a case by case basis we find that the increase in ELNB may be larger or smaller for moist- versus pseudoadiabatic ascent dependent on the subcloud-top thermodynamics of the original sounding and the substituted soundings. These complications explain the greater mean increase in ELNB for moist-adiabatic ascent for many cases. Although there are clear differences in the estimated entrainment rates and

TABLE 1. Summary of the sensitivity analysis to the type of ascent that is assumed. The properties of the parcel at the surface are assumed to be equal to the state of the atmosphere at 1000 mb. The substitutions are defined as follows: ExT, temperature profile from sounding with low stability near freezing level; ExRH, RH profile from sounding with the high midlevel relative humidity; ClimT, climatological temperature profile; and ClimRH, climatological RH profile. The number increase column gives the number of soundings that show an increase in the ELNB after each substitution compared to the no-substitution calculation.

Parcel ascent type	Substitutions	No. of increase	Mean (median) increase (km)	No. of ELNB $>$ 9 km
Pseudo	ExT	39	1.04 (0.88)	1
	ExRH	66	6.81 (6.94)	64
	ClimT	46	1.44 (1.14)	3
	ClimRH	22	2.88 (1.85)	5
Moist	ExT	32	1.37 (1.12)	7
	ExRH	67	7.51 (7.84)	60
	ClimT	33	2.48 (1.28)	8
	ClimRH	24	3.22 (2.67)	7

TABLE 2. Summary of the sensitivity analysis to initial parcel properties. The parcel ascent type may be either pseudo or moist adiabatic. The surface parcel description is defined as follows: B, the properties are defined by the lowest sounding level; C, surface parcel properties defined by the median over the lowest 1 km. Other columns are the same as those defined in Table 1.

Parcel ascent type	Surface parcel description	Substitutions	No. of increase	Mean (median) increase (km)	No. of ELNB > 9 km
Pseudo	B	ExT	54	1.24 (1.14)	1
	B	ExRH	67	6.51 (6.57)	65
	B	ClimT	36	0.97 (0.83)	2
	B	ClimRH	14	1.51 (0.96)	1
	C	ExT	40	0.91 (0.75)	0
	C	ExRH	66	6.43 (6.45)	64
	C	ClimT	51	1.48 (1.20)	5
	C	ClimRH	18	2.44 (1.72)	4
Moist	B	ExT	27	1.00 (0.66)	0
	B	ExRH	66	6.66 (7.16)	57
	B	ClimT	26	1.26 (1.02)	1
	B	ClimRH	20	2.95 (1.86)	4
	C	ExT	48	1.80 (1.50)	2
	C	ExRH	66	6.33 (6.50)	53
	C	ClimT	40	2.31 (1.57)	7
	C	ClimRH	20	2.17 (1.36)	2

subsequent ELNB, our general conclusions remain valid. The substitution of the extreme RH profiles still results in the only significant change in calculated values of the ELNB.

b. Initial parcel properties

Brown and Zhang (1997) use simple parcel theory and radiosonde data from TOGA COARE to investigate how the midtropospheric moisture affects the distribution of cloud-top heights. They emphasize that there is uncertainty in their calculations due to the assumption of the level of origin for a convective parcel of air. Consistent with the work of Brown and Zhang (1997) our initial analysis defines convective parcels as rising from the 1000-hPa level (we will refer to this as initial parcel property case A). We test the sensitivity of our calculations and results by repeating our analysis by defining the origin of the convective parcels using the properties defined by the lowest sonde observation (B) or the median of the lowest 1 km (C). The first choice represents a parcel rising from the surface (Renno and Williams 1995) while the second represents an average boundary layer parcel and could be thought of as representing parcels rising from a variety of levels in the boundary layer (Mapes 1993).

For pseudoadiabatic ascent the entrainment rates for parcels with initial properties B range between 1% and 68% km^{-1} (same as A) with relative differences ranging from −10% to 5% km^{-1} over the 67 cases. If we use description C, the range of entrainment rates tightens to 2%–65% km^{-1} with a relative difference compared to description A between −1% and 11% km^{-1}. We find similar results for moist-adiabatic ascent where entrainment rates for parcels with initial characteristics defined by B range between 1% and 42% km^{-1} (compared to 1%–43% km^{-1} for A) with relative differences from −16% to 10% km^{-1}. For initial parcel description C the entrainment rates vary from 1% to 38% km^{-1} with relative differences compared to description A between −3% and 13% km^{-1}.

Using these different representations of the surface parcel properties and the corresponding entrainment rate, we once again substitute the extreme temperature and moisture profiles for each congestus case and evaluate the impact on the ELNB. Table 2 summarizes the results for initial parcel descriptions B and C (for both pseudo- and moist-adiabatic assumptions) and can be compared to Table 1, which shows the same quantities for initial parcel description A. Table 2 shows that regardless of the type of ascent that is assumed (moist or pseudoadiabatic) and the assumption of the level of origin for the convective parcel, the largest mean increase in ELNB and the greatest number of ELNB values greater than 9 km occur for the substitution of the sounding with high midlevel RH. Of all the combinations of parcel ascent type, surface parcel description, and thermodynamic substitutions, only the cases where the extreme relative humidity (ExRH) are substituted are there greater than eight cases where the ELNB is greater than 9 km with a mean increase in the ELNB > 2.95 km. For the ExRH substitutions there are at least 60 (of a possible 67) cases with ELNB > 9 km and the mean increase in ELNB ranges from 6.43 to 7.51 km. For any combination not including the substitution of

the extreme relative humidity profile, there are often increases in the ELNB (column 4 in Table 2) but they are generally small (column 5 in Table 2) and do not reach deep convective levels (column 6 in Table 2). Therefore, our general conclusion, that the midlevel relative humidity plays a more important role in limiting convective cloud-top heights, is robust.

c. Vertical profile of entrainment rate

In the initial analysis we assumed that the entrainment rate σ is constant with height (cf. Brown and Zhang 1997) for simplicity and because there is little known about the vertical profile of entrainment rate. Entrainment in an individual cloud likely depends on a number of different factors including the size, vertical velocity, and thermodynamic properties of the rising parcel. From a GCM standpoint, entrainment rate is a bulk quantity characterizing an ensemble of updrafts present simultaneously within a large-scale region similar to a GCM grid box. Subgrid variability in the boundary layer thermodynamic properties due to turbulence, previous downdrafts, etc., and in free-troposphere humidity due to detrainment from previous updrafts, guarantee that a range of cloud-top heights will exist for other congestus clouds in the vicinity of the one sampled at Nauru at a given time. For example, we inferred instantaneous spatial variability in congestus heights over a 200 km × 200 km region including Nauru using infrared geostationary satellite images acquired within 15 min of a subset of 25 of our congestus cases. The mean standard deviation of congestus heights within a given large-scale scene is ~1.4 km, with the satellite mean congestus heights being on average ~0.8 km lower than the mean congestus heights at Nauru. This variability translates into ~10% scatter in entrainment rates in Fig. 4 and in the results to follow. This limits our ability to diagnose large-scale controls on entrainment and thus our results should only be viewed in a statistical sense.

Several modeling studies have investigated the vertical profiles of entrainment. Bretherton and Smolarkiewicz (1989) conclude that the entrainment depends on the vertical gradient of cloud buoyancy with entrainment occurring when the cloud buoyancy increases with height. Lin and Arakawa (1997) use output from a cloud resolving model and find that the entrainment is maximum near cloud base and cloud top. Lin (1999) uses a cloud resolving model to study an ensemble of deep convective clouds and finds that the entrainment tends to decrease through the depth of the cloud as a function of the cloud buoyancy. Gregory (2001) links entrainment rate to buoyant production of vertical kinetic energy but argues that his formulation implies a decrease in entrainment with height analogous to that found by Lin.

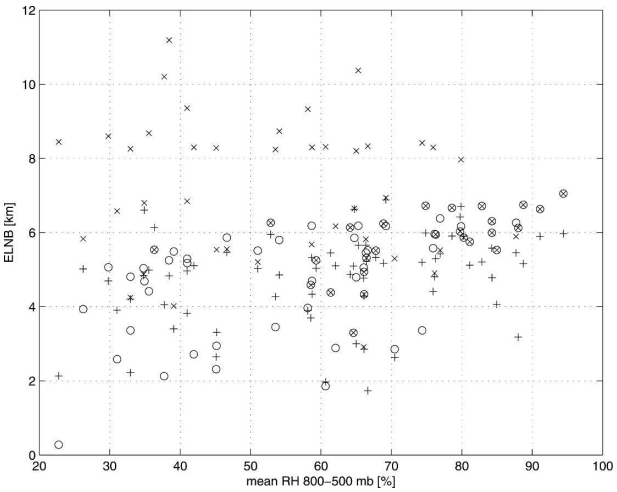

FIG. 8. Same as in Fig. 6b but with entrainment rate varying with height as a function of parcel buoyancy.

Because the study by Lin (1999) simulated clouds similar to those in this study, we use his parameterization of entrainment rate as a function of cloud buoyancy to test the sensitivity of our findings to a height-varying entrainment rate. We parameterize the entrainment rate as a function of buoyancy expressed by

$$\sigma = \lambda B^{-\alpha}, \tag{2}$$

where λ and α are parameters to be determined and B is the parcel buoyancy defined as

$$B = g\left(\frac{T_{vp} - T_v}{Tv}\right). \tag{3}$$

We use $\alpha = 1.27$, which is the average value for the four model runs done by Lin (1999) and then follow an algorithm similar to our constant entrainment calculations by increasing λ from zero until the ELNB is equal to or less than the ARSCL cloud-top height. For this set of calculations we assume pseudoadiabatic ascent and set the surface parcel characteristics equal to the 1000-hPa values (A).

The results of this sensitivity analysis are summarized in Fig. 8. Compared to entrainment rate, height-varying entrainment rate results in a similar pattern of ELNB increasing to deep convective levels mainly via the substitution of an RH profile with a moist midlevel; however, a much smaller portion of the cases extend to deep convective levels (only 5, although if we choose 8 km as the deep convection threshold this number increases to 20). This suggests that the midlevel relative humidity is still the most important of the factors tested

in this study for limiting convective cloud-top heights; however, there is also a buoyancy threshold in determining the cases that will extend to deep convective levels.

d. Glaciation of hydrometeors

Zuidema (1998) shows that cumulus congestus that overshoot the 0°C level may glaciate, causing an increase in parcel buoyancy due to the release of the latent heat of fusion. This increase in parcel buoyancy may be sufficient to allow the clouds to grow to deep convective depths. To account for this contribution, we have repeated our calculations including the freezing of hydrometeors for moist-adiabatic ascent, with the initial parcel properties defined by the 1000-mb level. For simplicity we assume that all liquid water in the parcel freezes instantly once the parcel rises above the freezing level. We estimate a new entrainment rate and go through our substitution exercise. The impact of including freezing in our parcel model is that our estimated entrainment rates are increased (i.e., the increased buoyancy upon freezing is offset by a larger entrainment rate) by 2%–41% km^{-1}. Using these new entrainment rates in the substitution exercise we find that for the cases showing an increase in the ELNB the mean (median) magnitude of those increases and the number of cases where the ELNB increases to greater than 9 km are virtually identical to the numbers shown in Table 1.

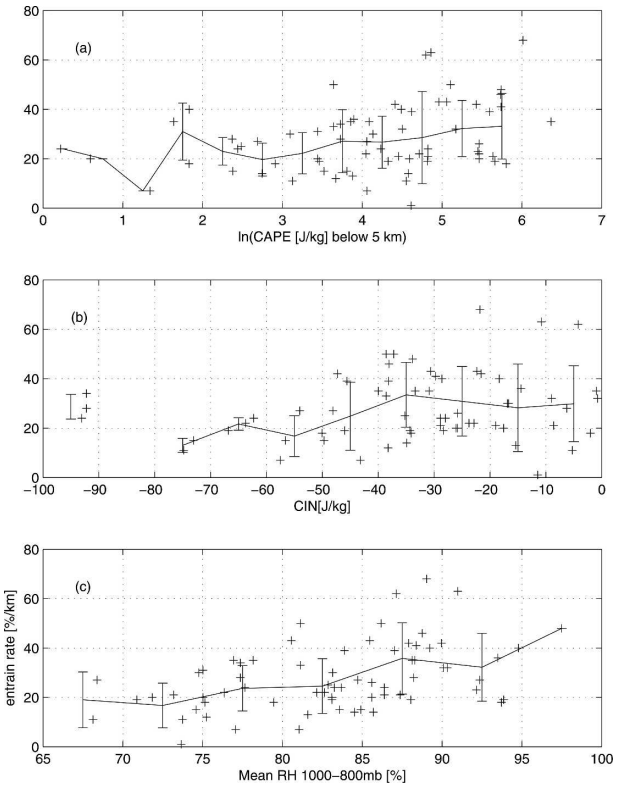

FIG. 9. Entrainment rate as a function of (a) ln (CAPE below 5 km), (b) CIN, and (c) 1000–800-hPa mean RH. The solid line represents the mean entrainment rate in appropriately sized bins for each variable with the standard deviation in each bin noted by the error bars.

6. Environmental parameters affecting entrainment rate

Our analysis lends itself to investigating links between the characteristics of the large-scale environment and the entrainment rate for the cumulus congestus cases in this study. Figure 9 shows scatterplots of several candidates that may play a role in determining the entrainment rates. We have included the mean and standard deviation for appropriately sized bins in each plot. Entrainment rate tends to increase with increasing low-level CAPE, decreasing magnitude of convective inhibition (CIN), and increasing low-level relative humidity but there is a great deal of scatter. The relationships we see are consistent with the idea that entrainment is related to the buoyant production of turbulent kinetic energy.

To better understand the relations between the various parameters, we perform a regression analysis to determine the percentage of the variance in entrainment rate that can be accounted for by each variable. Given that we observe an individual cloud, rather than a population of clouds within a larger-scale area whose own evolution influences the thermodynamic structure, and utilize a nonsimultaneous sounding (albeit the nearest one) to analyze it, we can only hope to explain part of the implied variance in entrainment rate. Table 3 shows that the greatest portion of the variance in the estimated entrainment rates is explained by the CAPE and RH profile. However, these variables explain less than one-third of the total variance (column 1). We tested the sensitivity of these results to the separation time between the sounding launch and the congestus cloud observation by including only cases where this time was less than 3 or 1 h. This analysis showed that a decrease from 6 to 1 h resulted in a change from 26% to 90% in the maximum amount of variance that could be explained. This suggests that low-level CAPE and RH explain most of the variance in the cumulus congestus entrainment rates and that small-scale variability in the atmospheric thermodynamic structure must be sampled in order to describe the entrainment. Additional variance may be associated with our neglect of height-varying σ in this calculation or by high-frequency spa-

TABLE 3. Results of the regression analysis of several candidate atmospheric quantities and the estimated entrainment rates.

Variable(s)	R^2 (sounding within 6 h)	R^2 (sounding within 3 h)	R^2 (sounding within 1 h)
CAPE below 5 km	0.12	0.53	0.85
CIN	0.03	0.01	0.04
Mean RH (2–4 km)	0.20	0.20	0.19
Mean RH (5–7 km)	0.18	0.28	0.19
CAPE, mean RH (2–4 km)	0.26	0.58	0.90
Wind shear (surface–700 hPa)	0.002	0.004	0.022
Max buoyancy $<$ 5 km	0.19	0.22	0.29

tial and temporal variability of the thermodynamic structure that cannot be captured by a sparse sample of soundings in one location. One possible source of this type of high-frequency variability in the atmospheric thermodynamic structure is planetary boundary layer rolls (Weckwerth et al. 1996).

7. Summary and conclusions

In this study we have used observations from an ARM surface-based remote sensing site coupled with a simple parcel model in order to better understand the factors that limit the vertical development of cumulus congestus clouds in the Tropics. We have tested several different hypotheses concerning the role of atmospheric thermodynamic structure in this development. Our results indicate that at Nauru Island a drying of the midtroposphere is a more likely to be responsible for limiting congestus cloud-top heights compared to a stabilizing of the freezing level. This result confirms the results of Brown and Zhang (1997), Redelsperger et al. (2002), and Takemi et al. (2004) who showed that low values of midlevel RH in the tropical western Pacific were sufficient to suppress convection. We have generalized this result to account for physically estimated entrainment rates and varying assumptions of parcel thermodynamics using observations collected over 3 yr at the ARM Nauru Island climate research facility. This conclusion is based only on observations from Nauru and we suspect that freezing-level stability could play a more prominent role in regions where deep convection and therefore extended anvil cloud decks are more prevalent. Our analysis required the estimation of entrainment rates for each cumulus congestus case. We investigate the relationship between several candidate atmospheric properties and the magnitude of the entrainment rate. A regression analysis indicates that, of the properties chosen, low-level CAPE and the RH profile account for the largest portion of the variance in entrainment rate. If we limit this analysis to cases where there is a sounding within the hour preceding the cumulus congestus observation (thus minimzing the impacts of small scale fluctuations in the atmospheric thermodynamics), then these quantities can explain as much as 90% of the variance in the estimated entrainment rates.

Small-scale spatial and temporal variability in thermodynamic structure that cannot be captured by the infrequent soundings at Nauru may account for a good part of the remaining variance; that is, we have no way of diagnosing the effects of localized boundary layer moist patches or cold pools or remnant free-troposphere moist layers from prior convective events. We also have no way of differentiating thermals of different size that will experience different degrees of entrainment. These limitations are a reminder that cumulus parameterizations in GCMs can never be expected to successfully simulate the details of individual convection case studies over short time periods, but rather must be evaluated on the basis of the statistics they produce over large numbers of events. Our results do suggest that, in a statistical sense, parameterizations that relate entrainment rate to the buoyant production of turbulent kinetic energy may have some predictive capability.

Acknowledgments. This work was supported by the U.S. Department of Energy's Atmospheric Radiation Measurement Program. We thank Audrey Wolf for her help with the satellite data analysis. We would also like to thank two anonymous reviewers whose comments and suggestions have been very helpful.

REFERENCES

Blanchard, D. O., 1998: Assessing the vertical distribution of convective available potential energy. *Wea. Forecasting,* **13,** 870–877.

Bretherton, C. S., and P. K. Smolarkiewicz, 1989: Gravity waves, compensating subsidence and detrainment around cumulus clouds. *J. Atmos. Sci.,* **46,** 740–759.

Brown, R. G., and C. Zhang, 1997: Variability of midtropospheric moisture and its effect on cloud-top height distribution during TOGA COARE. *J. Atmos. Sci.,* **54,** 2760–2774.

Clothiaux, E. E., T. P. Ackerman, G. G. Mace, K. P. Moran, R. T.

Marchand, M. A. Miller, and B. E. Martner, 2000: Objective determination of cloud heights and radar reflectivities using a combination of active remote sensors at the ARM CART sites. *J. Appl. Meteor.,* **39,** 645–665.

Del Genio, A. D., W. Kovari, M.-S. Yao, and J. Jonas, 2005: Cumulus microphysics and climate sensitivity. *J. Climate,* **18,** 2376–2387.

DeMott, C. A., and S. A. Rutledge, 1998: The vertical structure of TOGA COARE convection. Part II: Modulating influences and implications for diabatic heating. *J. Atmos. Sci.,* **55,** 2748–2762.

Derbyshire, S. H., I. Beau, P. Bechtold, J.-Y. Grandpeix, J.-M. Pirou, J.-L. Redelsperger, and P. M. M. Soares, 2004: Sensitivity of moist convection to environmental humidity. *Quart. J. Roy. Meteor. Soc.,* **130,** 3055–3079.

Gregory, D., 2001: Estimation of entrainment rate in simple models of convective clouds. *Quart. J. Roy. Meteor. Soc.,* **127,** 53–72.

Guichard, F., D. Parsons, and E. Miller, 2000: Thermodynamic and radiative impact of the correction of sounding humidity bias in the Tropics. *J. Climate,* **13,** 3611–3624.

——, and Coauthors, 2004: Modelling the diurnal cycle of deep precipitating convection over land with cloud-resolving models and single-column models. *Quart. J. Roy. Meteor. Soc.,* **130,** 3139–3172.

Houze, R. A., Jr., 1989: Observed structure of mesoscale convective systems and implications for large-scale heating. *Quart. J. Roy. Meteor. Soc.,* **115,** 425–461.

——, and D. D. Churchill, 1987: Mesoscale organization and cloud microphysics in a Bay of Bengal depression. *J. Atmos. Sci.,* **44,** 1845–1867.

Johnson, R. H., T. M. Rickenbach, S. A. Rutledge, P. E. Ciesielelki, and W. H. Shubert, 1999: Trimodal characteristics of tropical convection. *J. Climate,* **12,** 2397–2418.

Kollias, P., B. A. Albrecht, and F. D. Marks Jr., 2003: Cloud radar observations of vertical drafts and microphysics in convective rain. *J. Geophys. Res.,* **108,** 4053, doi:10.1029/2001JD002033.

——, C. Williams, and B. A. Albrecht, 2006: Statiform precipitation observations by 3-GHz and 94-GHz doppler radars. *Quart. J. Roy. Meteor. Soc.,* in press.

Lin, C., 1999: Some bulk properties of cumulus ensembles simulated by a cloud-resolving model. Part II: Entrainment profiles. *J. Atmos. Sci.,* **56,** 3736–3748.

——, and A. Arakawa, 1997: The macroscopic entrainment processes of simulated cumulus ensemble. Part I: Entrainment sources. *J. Atmos. Sci.,* **54,** 1027–1043.

Lucas, C., E. J. Zipser, and M. A. LeMone, 1994: Vertical velocity in oceanic convection off tropical Australia. *J. Atmos. Sci.,* **51,** 3183–3193.

Mapes, B. E., 1993: Gregarious tropical convection. *J. Atmos. Sci.,* **50,** 2026–2037.

——, and P. Zuidema, 1996: Radiative-dynamical consequences of dry tongues in the tropical tropopause. *J. Atmos. Sci.,* **53,** 620–638.

Mather, J. H., T. P. Ackerman, M. P. Jensen, and W. E. Clements, 1998: Characteristics of the atmospheric state and the surface radiation budget at the tropical western Pacific ARM site. *Geophys. Res. Lett.,* **25,** 4513–4516.

McFarquhar, G. M., and A. J. Heymsfield, 1996: Microphysical characteristics of three anvils sampled during the Central Equatorial Pacific Experiment (CEPEX). *J. Atmos. Sci.,* **53,** 2401–2423.

Numaguti, A., R. Oki, K. Nakamura, K. Tsuboki, N. Misawa, T. Asai, and Y.-M. Kodma, 1995: 4–5-day-period variation and low-level dry air observed in the equatorial western Pacific during the TOGA-COARE IOP. *J. Meteor. Soc. Japan,* **73,** 267–290.

Redelsperger, J.-L., D. B. Parsons, and F. Guichard, 2002: Recovery processes and factors limiting cloud-top height following the arrival of a dry intrusion observed during TOGA COARE. *J. Atmos. Sci.,* **59,** 2438–2457.

Renno, N. O., and E. R. Williams, 1995: Quasi-Lagrangian measurements in convective boundary layer plumes and their implications for the calculation of CAPE. *Mon. Wea. Rev.,* **123,** 2733–2742.

Sherwood, S. C., 1999: Convective precursors and predictability in the tropical Western Pacific. *Mon. Wea. Rev.,* **127,** 2977–2991.

Sheu, R.-S., and G. Liu, 1995: Atmospheric humidity variations associated with westerly wind bursts during Tropical Ocean Global Atmosphere (TOGA) Coupled Ocean Atmosphere Response Experiment (COARE). *J. Geophys. Res.,* **100,** 25 759–25 768.

Takemi, T., O. Hirayama, and C. Liu, 2004: Factors responsible for the vertical development of tropical oceanic cumulus convection. *Geophys. Res. Lett.,* **31,** L11109, doi:10.1029/2004GL020225.

Wang, J., H. L. Cole, D. J. Carlson, E. R. Miller, K. Beierle, A. Paukkunen, and T. K. Lane, 2002: Corrections of humidity measurement errors from the Vaisala RS80 radiosonde—Application to TOGA COARE data. *J. Atmos. Oceanic Technol.,* **19,** 981–1002.

Weckwerth, T. M., J. W. Wilson, and R. M. Wakimoto, 1996: Thermodynamic variability within the convective boundary layer due to horizontal convective rolls. *Mon. Wea. Rev.,* **124,** 769–784.

Westwater, E. R., B. B. Stankov, D. Cimini, Y. Han, J. A. Shaw, B. M. Lesht, and C. N. Long, 2003: Radiosonde humidity soundings and microwave radiometers during Nauru99. *J. Atmos. Oceanic Technol.,* **20,** 953–971.

Xu, K.-M., and K. A. Emanuel, 1989: Is the tropical atmosphere conditionally unstable? *Mon. Wea. Rev.,* **117,** 1471–1479.

Yoneyama, K., and D. B. Parsons, 1999: A proposed mechanism for the intrusion of dry air into the tropical western Pacific region. *J. Atmos. Sci.,* **56,** 1524–1546.

Zuidema, P., 1998: The 600–800-mb minimum in tropical cloudiness observed during TOGA COARE. *J. Atmos. Sci.,* **55,** 2220–2228.